Available online at www.sciencedirect.com
SCIENCE DIRECT®
Journal of Sound and Vibration 280 (2005) 681–698
JOURNAL OF SOUND AND VIBRATION
www.elsevier.com/locate/jsvi

A simplified numerical model for a plate backed by a thin foam layer in the low frequency range

L. Jaouen[a,b,*], B. Brouard[a], N. Atalla[b], C. Langlois[b]

[a] *Laboratoire d'Acoustique de l'Université du Maine, UMR CNRS 6613, 72085 Le Mans Cedex, France*
[b] *Groupe d'Acoustique de l'Université de Sherbrooke, Sherbrooke, Québec, Canada J1K 2R1*

Received 20 March 2003; accepted 12 December 2003

Abstract

This paper presents a simplified numerical model based on a hierarchical trigonometric functions set to predict the low frequency vibration behaviour of a plate backed by a thin foam layer. The base metal plate is excited in bending vibrations with a point load and can have various boundary conditions. The poro-elastic layer is modelled using the mixed displacement–pressure formulation of the Biot–Allard's theory. The base plate and the solid phase of the porous medium are described as an equivalent visco-elastic plate. The poro-elastic's fluid phase is coupled with the equivalent plate displacements.

Comparisons with complete three-dimensional poro-elastic finite element solutions and experimental data are presented to define a domain of validation for the proposed simplified model.

1. Introduction

Multilayered structures including poro-elastic materials, like polymer foams, are widely used for sound absorption and vibration damping in buildings construction and in the transport industries. For a quick analysis of some vibro-acoustic or transmission phenomena, a simple prediction involving a metal plate backed by a poro-elastic material can be used.

Prediction of the vibro-acoustic behaviour of poro-elastic materials can be done using the Biot–Allard's theory [1,2]. This theory describes the poro-elastic material as two phases coupled in time and space. The poro-elastic material is described with five geometrical parameters: the porosity ϕ, the flow resistivity σ, the tortuosity α_∞, the viscous characteristic length Λ, the thermal

*Corresponding author. Tel.: +33-2-43-833667; fax: +33-2-43-833520.
E-mail address: luc.jaouen@univ-lemans.fr (L. Jaouen).

0022-460X/$ - see front matter © 2003 Elsevier Ltd. All rights reserved.
doi:10.1016/j.jsv.2003.12.038

characteristic length Λ' and the mechanical parameters of the skeleton and the saturating fluid's properties.

Evaluation of the performance of finite size multilayered structures involving porous media is usually done with complete three-dimensional poro-elastic finite element models which lead to significant computation time and memory usage. However, some practical configurations can be more easily described by using assumptions about the porous material behaviour.

Investigating the dissipation mechanisms in a thin foam layer bonded onto a simply supported aluminium plate, Dauchez et al. [3] found that structural damping of the solid phase is the major dissipative mechanism occurring within the material for stiff foams at low frequencies. Consequently, neglecting the material's fluid phase, these authors proposed to use an equivalent visco-elastic plate model for the very first modes. This model, which does not include any viscous dissipation in the porous medium is almost suitable for low resistivity materials. Rigobert [4] tried to extend this work to the case of highly resistive foams and fibrous materials, for which the viscous dissipation cannot be neglected any longer. In this new model, a detailed three-dimensional finite element based solution of the problem is required to determine a modified structural damping coefficient of the equivalent plate accounting for structural and viscous dissipation occurring in the porous layer. Although the method gives good results, it has no advantage over a complete calculation.

Etchessahar et al. [5] have recently presented a model based on the displacement-pressure formulation of the Biot–Allard theory [6] to simulate bending vibrations of thin simply-supported or clamped stand-alone poro-elastic plates. This model's advantage is a rigorous description of the poro-elastic medium with its two phases and interactions between these phases. Experiments have shown that this model is relevant to predict the first resonances of high density porous materials. The experimental realization is however difficult to set up for a wide variety of materials.

In this paper, a new model is introduced, built on the conclusions of Dauchez et al. [3] and Etchessahar et al. [5], to simulate the vibration behaviour of an elastic plate backed by an isotropic polymeric foam (Fig. 1). The porous layer is described by the mixed displacement-pressure formulation of the Biot–Allard theory [6]. The base plate and the porous solid phase are modelled as an equivalent visco-elastic plate and assumed admissible functions are used to describe the fluid phase pressure. The Rayleigh–Ritz method using a trigonometric functions set

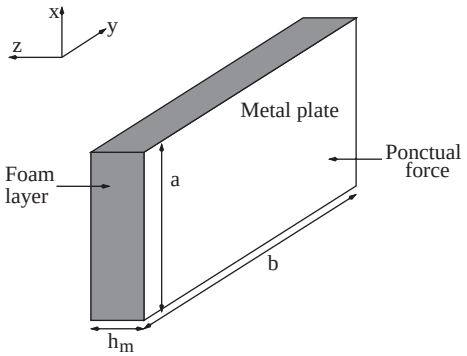

Fig. 1. Aluminium plate under concentrated load and backed by a foam.

[7] is employed to solve the variational equations of motion. Thus, various boundary conditions can be applied to the base plate: simply-supported, clamped or free edges.

2. Theoretical background

This section presents the mixed displacement–pressure formulation of the Biot–Allard's theory [1,2,6] with corrections for viscous and thermal dissipative effects introduced by Johnson et al. [8] and Champoux et al. [9] respectively. Each dissipation mechanism is briefly discussed before introducing the variational formulation for a plate-porous system in bending vibrations.

In the following, the $\sim$ symbol denotes a frequency dependent quantity.

2.1. The Biot–Allard's poroelastic model

Assuming a harmonic time dependence of the form $e^{+j\omega t}$, the coupled volumetric equations of equilibrium between the porous two phases as functions of the solid phase displacement field $\mathbf{u}$ and the fluid phase pore pressure p is [6]:

$$\operatorname{div} \hat{\boldsymbol{\sigma}}^s(\mathbf{u}) + \omega^2 \tilde{\rho}\, \mathbf{u} = -\tilde{\gamma} \boldsymbol{\nabla} p, \tag{1}$$

$$\Delta p + \omega^2 \frac{\tilde{\rho}_{22}}{\tilde{R}} p = \omega^2 \tilde{\gamma} \frac{\tilde{\rho}_{22}}{\phi^2} \operatorname{div}\, \mathbf{u}. \tag{2}$$

In the above equations, $\hat{\boldsymbol{\sigma}}^s$ is the stress tensor of the material's solid phase in vacuum. $\tilde{\rho}$ is the dynamic effective density of the porous material defined as

$$\tilde{\rho}(\omega) = \tilde{\rho}_{11} - \frac{\tilde{\rho}_{12}^2}{\tilde{\rho}_{22}}, \tag{3}$$

where $\tilde{\rho}_{12}$, $\tilde{\rho}_{11}$ and $\tilde{\rho}_{22}$ are complex dynamic densities considering viscous effects:

$$\tilde{\rho}_{12}(\omega) = \rho_{12} - \frac{\tilde{b}}{j\omega}, \tag{4}$$

$$\tilde{\rho}_{11}(\omega) = \rho_{11} + \frac{\tilde{b}}{j\omega}, \tag{5}$$

$$\tilde{\rho}_{22}(\omega) = \rho_{22} + \frac{\tilde{b}}{j\omega}, \tag{6}$$

with

$$\rho_{12} = -\phi \rho_0 (\alpha_\infty - 1), \tag{7}$$

$$\rho_{11} = \rho_1 - \rho_{12}, \tag{8}$$

$$\rho_{22} = \rho_2 - \rho_{12}, \tag{9}$$

$$\tilde{b}(\omega) = \phi^2 \sigma \tilde{G}(\omega), \tag{10}$$

$$j = \sqrt{-1}. \tag{11}$$

ρ_1 and ρ_2 are the solid and fluid phase densities described as functions of the medium's porosity ϕ, the density of the material which constitutes the skeleton ρ_s and the fluid density ρ_0 (1.23 kg m^{-3} at 18°C under 1.013×10^5 Pa):

$$\rho_1 = (1-\phi)\rho_s, \tag{12}$$

$$\rho_2 = \phi\rho_0. \tag{13}$$

$\tilde{b}$ is a complex and frequency dependent viscous damping coefficient function of a viscosity correction factor $\tilde{G}$ representing the fact that the pore flow departs from a Poiseuille's flow when the angular frequency ω increases. The expression of $\tilde{G}$ according to the Johnson et al. model [8] is

$$\tilde{G}(\omega) = \sqrt{1 + \mathrm{j}\frac{4\alpha_\infty^2 \mu\rho_0\omega}{\sigma^2\Lambda^2\phi^2}}, \tag{14}$$

where μ is the viscosity of air (1.84 N s m^{-2} at 18°C under 1.013×10^5 Pa).

$\tilde{\gamma}$, $\tilde{R}$, introduced in Eqs. (1) and (2), and $\tilde{Q}$ are frequency dependent terms which can be written as [10]:

$$\tilde{\gamma}(\omega) = \frac{\rho_0}{\tilde{\rho}_{22}}\phi^2 - 1, \tag{15}$$

$$\tilde{R}(\omega) = \phi\tilde{K}_e(\omega), \tag{16}$$

and

$$\tilde{Q}(\omega) = (1-\phi)\tilde{K}_e(\omega) \tag{17}$$

with

$$\tilde{K}_e(\omega) = \frac{\gamma P_0}{\gamma - (\gamma-1)\left[1 + \dfrac{8\mu}{\mathrm{j}\Lambda'^2 B^2\omega\rho_0}\tilde{G}'\right]^{-1}}. \tag{18}$$

$\tilde{K}_e$ is the air bulk modulus accounting for thermal dissipation between the two porous phases [2]. Note that these expressions assume that the bulk modulus of the foam is small compared to the bulk modulus of the material from which the skeleton is made; which is valid for the majority of foams used in acoustics. P_0 is the atmospheric pressure, γ the ratio of specific heats (its value is 1.4 for air at 18°C under 1.013×10^5 Pa), B^2 is the Prandtl number ($B^2 = 0.71$ at 18°C under 1.013×10^5 Pa) and finally $\tilde{G}'$ is a thermal correction factor [9] similar to $\tilde{G}$ introduced earlier:

$$\tilde{G}' = \sqrt{1 + \mathrm{j}\frac{\Lambda'^2 B^2\rho_0\omega}{16\mu}}. \tag{19}$$

The right hand side members in both equations (1) and (2) can be regarded as source terms. They couple the two phases dynamic responses. Setting these source terms to zero leads to an elastodynamic equation of the material in vacuum and a classical equivalent fluid (rigid skeleton [2]) equation respectively.

2.2. Dissipation mechanisms

Among the three dissipation mechanisms occurring within a porous layer: structural, viscous and thermal, the latter has been found negligible at low frequencies for typical polymeric foams of various thicknesses in plate-foam configurations [11]. Thus, no particular focus on thermal dissipation is done in this work.

2.2.1. Structural damping

Structural damping will be included in the present model using the complex modulus convention for each of the two layers:

$$\tilde{E}^*(\omega) = \tilde{E}(\omega)[1 + \mathrm{j}\tilde{\eta}(\omega)]. \tag{20}$$

In the above equation, * denotes a complex variable.

The structural damping $\tilde{\eta}$ can also be used to account for various dissipation phenomena such as the acoustic radiation and losses through the boundaries. However, these two dissipation mechanisms are neglected here (i.e., light fluid and lossless boundaries assumptions).

2.2.2. Viscous dissipation

For stiff polymer foams, structural damping is the major dissipative phenomenon at low frequencies [3]. As a consequence, it is assumed that the two layers system can be described as an equivalent viscous plate, the added viscous dissipation will be included in the present model using the foam's effective density $\tilde{\rho}$ [1,2] and assuming an admissible variation for the fluid phase pressure based on the boundary conditions at the plate-porous and porous-air interfaces.

2.2.3. Dissipated powers

Expressions of the dissipated powers which will be used to interpret the results are given in this section where Ω^m denotes the porous material volume and Im the imaginary part of a complex quantity. A definition of the power dissipated by structural effects inside the porous medium is

$$\Pi^s_{diss} = \tfrac{1}{2}\,\mathrm{Im}\left(\omega \int_{\Omega^m} \hat{\boldsymbol{\sigma}}^s(\mathbf{u}) : \boldsymbol{\varepsilon}^s(\mathbf{u})\mathrm{d}\Omega\right). \tag{21}$$

$\boldsymbol{\varepsilon}^s$ is the solid phase strain tensor.

Approximations of the powers dissipated by viscous and thermal effects when the ratio $\tilde{Q}/\tilde{R}$ can be considered real are respectively:

$$\Pi^v_{diss} = \tfrac{1}{2}\,\mathrm{Im}\left[-\omega^3 \int_{\Omega^m} \tilde{\rho}\mathbf{u}\cdot\mathbf{u}^*\,\mathrm{d}\Omega + \int_{\Omega^m} \frac{\phi^2}{\omega\tilde{\rho}_{22}} \boldsymbol{\nabla} p\cdot(\boldsymbol{\nabla} p)^*\,\mathrm{d}\Omega - 2\omega\tilde{\gamma}\int_{\Omega^m} \mathrm{Re}(\boldsymbol{\nabla} p\cdot\mathbf{u}^*)\mathrm{d}\Omega\right], \tag{22}$$

$$\Pi^t_{diss} = \tfrac{1}{2}\,\mathrm{Im}\left[-\omega \int_{\Omega^m} \frac{\phi^2}{\tilde{R}} p\cdot p^*\,\mathrm{d}\Omega\right]. \tag{23}$$

2.3. Variational formulation

In the following, the variational formulation for an elastic plate backed by a poro-elastic layer is described. The base plate is excited by a transverse point load of amplitude f_0 at position (x_0, y_0). The porous material is supposed to be perfectly bonded onto the plate.

2.3.1. Weak integral formulation

Below, superscripts p, m, s and f denote respectively a plate variable, a global porous variable, a material's solid or fluid phase related variable. Subscript n denotes a displacement normal to the plate plane. Ω^p, Ω^m and $\delta\Omega^p \cap \delta\Omega^m$ denote respectively the plate volume, the porous material volume and the plate-porous interface. $\boldsymbol{\varepsilon}^i$ and $\boldsymbol{\sigma}^i$ are strain and stress tensor of layer i.

Let δu and δp be, respectively, admissible variations of the solid phase displacements field $\mathbf{u}$ and the fluid phase pressure p. $\mathbf{U}^f$ is the displacement vector of the material's fluid phase. Assuming a harmonic time dependence of the form $e^{+j\omega t}$, the weak $(\mathbf{u}, p)$ integral formulation of the Biot's theory [1,12] is

$$\underbrace{\int_{\Omega^p} \boldsymbol{\sigma}^p : \delta\boldsymbol{\varepsilon}^p \,\mathrm{d}\Omega - \rho^p\omega^2 \int_{\Omega^p} \mathbf{u}^p \cdot \delta\mathbf{u}^p \,\mathrm{d}\Omega}_{\text{plate domain}} + \underbrace{\int_{\Omega^m} \hat{\boldsymbol{\sigma}}^s : \delta\boldsymbol{\varepsilon}^s \,\mathrm{d}\Omega - \tilde{\rho}\omega^2 \int_{\Omega^m} \mathbf{u}^s \cdot \delta\mathbf{u}^s \,\mathrm{d}\Omega}_{\text{porous material's solid phase}}$$
$$+ \underbrace{\int_{\Omega^m} \left[\frac{\phi^2}{\omega^2\tilde{\rho}_{22}} \boldsymbol{\nabla} p \cdot \boldsymbol{\nabla}\delta p - \frac{\phi^2}{\tilde{R}} p\delta p\right] \mathrm{d}\Omega}_{\text{porous material's fluid phase}}$$
$$- \underbrace{\int_{\Omega^m} \left[\tilde{\gamma} + \phi\left(1 + \frac{\tilde{Q}}{\tilde{R}}\right)\right] \delta(\boldsymbol{\nabla} p \cdot \mathbf{u}^s)\mathrm{d}\Omega - \phi\left(1 + \frac{\tilde{Q}}{\tilde{R}}\right) \int_{\Omega^m} \delta(p \cdot \mathrm{div}(\mathbf{u}^s))\mathrm{d}\Omega}_{\text{coupling terms between the porous material's two phases}}$$
$$- \int_{\delta\Omega^p \cap \delta\Omega^m} (\boldsymbol{\sigma}^p \cdot \mathbf{n}^p) \cdot \delta\mathbf{u}^p \,\mathrm{d}S - \int_{\delta\Omega^p \cap \delta\Omega^m} (\boldsymbol{\sigma}^m \cdot \mathbf{n}^m) \cdot \delta\mathbf{u}^s \,\mathrm{d}S$$
$$- \int_{\delta\Omega^p \cap \delta\Omega^m} \phi(U_n^f - u_n^s)\delta p \,\mathrm{d}S = \int_{\delta\Omega^p} f_i \delta u_i \,\mathrm{d}S. \tag{24}$$

The relations to be satisfied at the interface between the elastic base plate and the porous medium are [12]:

$$\boldsymbol{\sigma}^p \cdot \mathbf{n}^p = -\boldsymbol{\sigma}^m \cdot \mathbf{n}^m, \tag{25}$$

$$\mathbf{u}^p = \mathbf{u}^m, \tag{26}$$

$$U_n^f - u_n^s = 0, \tag{27}$$

where $\mathbf{n}^p$ and $\mathbf{n}^m$ denote the exterior normals to the plate or the material domain.

The condition (25) ensures the continuity of the normal stresses (using the choosen mixed variational formulation, all the other associated boundary terms cancel out [12]). The second condition ensures the continuity of the displacement vectors between the two layers. And finally, the third equation (27) ensures the continuity of the relative mass flux vector across the boundary.

These conditions represent a perfect bond between the porous layer's solid phase and the plate and an impervious condition for the pore pressure at the plate-porous interface.

2.3.2. Displacement fields

The classical elastic thin plate theory [13] is used to describe the base plate displacement field. The neutral plan of the two layer system can be fixed to the mid plan of the plate, if a metal plate is considered, regardless of the difference in Young's moduli order between the plate and the foam. Thus for the plate we can write:

$$u_p(x,y,z,t) = -z\frac{\partial w}{\partial x}, \tag{28}$$

$$v_p(x,y,z,t) = -z\frac{\partial w}{\partial y}, \tag{29}$$

$$w_p(x,y,z,t) = w(x,y,t), \tag{30}$$

where u and v are the first order approximation of the plate's in-plane displacements and t denotes time.

The displacement field of the porous layer solid phase exhibits both bending and shear (cf. Fig. 2); the transverse displacement w is supposed to be the same for the two layers:

$$u_m(x,y,z,t) = -z\frac{\partial w}{\partial x} - \left(z - \frac{h_p}{2}\right)\psi_x(x,y,t), \tag{31}$$

$$v_m(x,y,z,t) = -z\frac{\partial w}{\partial y} - \left(z - \frac{h_p}{2}\right)\psi_y(x,y,t), \tag{32}$$

$$w_m(x,y,z,t) = w(x,y,t), \tag{33}$$

where ψ_x and ψ_y are the deviation angles due to shear strain.

2.3.3. Application of Hamilton's principle

The plate and the material's solid phase are supposed to be isotropic, homogeneous, rectangular of dimensions $a \times b$ and of uniform thicknesses h_p and h_m ($h_p, h_m \ll (a,b)$). Thus, using

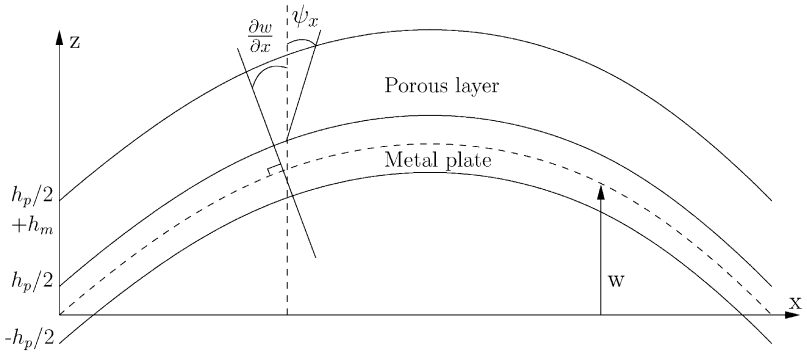

Fig. 2. Schema of the plate and material displacements.

Hamilton's principle, the third and fourth integrals of Eq. (24) become (see Ref. [3] for a detailed similar calculus):

$$\begin{aligned}
&\frac{1}{2}\int_{-a/2}^{a/2}\int_{-b/2}^{b/2}\left\{D_2\left[\left(\frac{\partial^2 w}{\partial x^2}\right)^2+\left(\frac{\partial^2 w}{\partial y^2}\right)^2+2\nu_m\frac{\partial^2 w}{\partial x^2}\frac{\partial^2 w}{\partial y^2}+2(1-\nu_m)\left(\frac{\partial^2 w}{\partial x\partial y}\right)^2\right]\right.\\
&+\ D_3\left[\left(\frac{\partial\psi_x}{\partial x}\right)^2+\left(\frac{\partial\psi_y}{\partial y}\right)^2+2\,\nu_m\frac{\partial\psi_x}{\partial x}\frac{\partial\psi_y}{\partial y}+\frac{1-\nu_m}{2}\left(\frac{\partial\psi_x}{\partial y}+\frac{\partial\psi_y}{\partial x}\right)^2\right]\\
&+2D_4\left[\left(\frac{\partial^2 w}{\partial x^2}\frac{\partial\psi_x}{\partial x}+\frac{\partial^2 w}{\partial y^2}\frac{\partial\psi_y}{\partial y}\right)+\nu_m\left(\frac{\partial^2 w}{\partial x^2}\frac{\partial\psi_y}{\partial y}+\frac{\partial^2 w}{\partial y^2}\frac{\partial\psi_x}{\partial x}\right)\right.\\
&\left.\left.+\ (1-\nu_m)\frac{\partial^2 w}{\partial x\partial y}\left(\frac{\partial\psi_x}{\partial y}+\frac{\partial\psi_y}{\partial x}\right)\right]+\ D_5[\psi_x^2+\psi_y^2]\right\}\mathrm{d}x\,\mathrm{d}y\\
&-\tfrac{1}{2}\tilde{\rho}\omega^2\int_{-a/2}^{a/2}\int_{-b/2}^{b/2}\int_{z_1}^{z_2}\left(w^2+\left\{z\frac{\partial w}{\partial x}+\left(z-\frac{h_p}{2}\right)\psi_x\right\}^2\right.\\
&\left.+\left\{z\frac{\partial w}{\partial y}+\left(z-\frac{h_p}{2}\right)\psi_y\right\}^2\right)\mathrm{d}x\,\mathrm{d}y\,\mathrm{d}z,
\end{aligned}\tag{34}$$

where the D_i denote the following integrals:

$$D_2=\frac{E_m}{(1-\nu_m^2)}\int_{z_1}^{z_2}z^2\,\mathrm{d}z,\tag{35}$$

$$D_3=\frac{E_m}{(1-\nu_m^2)}\int_{z_1}^{z_2}\left(z-\frac{h_p}{2}\right)^2\mathrm{d}z,\tag{36}$$

$$D_4=\frac{E_m}{(1-\nu_m^2)}\int_{z_1}^{z_2}z\left(z-\frac{h_p}{2}\right)\mathrm{d}z,\tag{37}$$

$$D_5=\frac{\kappa^2 E_m}{2(1+\nu_m)}\int_{z_1}^{z_2}\mathrm{d}z,\tag{38}$$

E_m and ν_m are the Young's modulus and the Poisson ratio of the porous medium, $z_1=h_p/2$, $z_2=(h_p/2)+h_m$ and κ^2 is the Mindlin's correction factor [14] taken as $\frac{5}{6}$.

The first two integrals of Eq. (24) have the same form, one might only change the integration domain and rigidities to fit the first layer's boundaries.

The integral related to the material's fluid phase is

$$\frac{1}{2}\frac{\phi^2}{\omega^2\tilde{\rho}_{22}}\int_{\Omega^m}\left[\left(\frac{\partial p}{\partial x}\right)^2+\left(\frac{\partial p}{\partial y}\right)^2+\left(\frac{\partial p}{\partial z}\right)^2\right]\mathrm{d}\Omega-\frac{1}{2}\frac{\phi^2}{\tilde{R}}\int_{\Omega^m}p^2\,\mathrm{d}\Omega\tag{39}$$

and the coupling terms can be written:

$$(\tilde{\gamma}+1)\int_{\Omega^m}\left[\frac{\partial p}{\partial x}\left(z\frac{\partial w}{\partial x}+\left(z-\frac{h_p}{2}\right)\psi_x\right)+\frac{\partial p}{\partial y}\left(z\frac{\partial w}{\partial y}+\left(z-\frac{h_p}{2}\right)\psi_y\right)-\frac{\partial p}{\partial z}w\right]\mathrm{d}\Omega, \tag{40}$$

$$\int_{\Omega^m} p\left(z\frac{\partial^2 w}{\partial x^2}+\left(z-\frac{h_p}{2}\right)\frac{\partial \psi_x}{\partial x}+z\frac{\partial^2 w}{\partial y^2}+\left(z-\frac{h_p}{2}\right)\frac{\partial \psi_y}{\partial y}\right)\mathrm{d}\Omega, \tag{41}$$

noting that, from (18) and (16), $\phi\tilde{Q}/\tilde{R}=(1-\phi)$.

Finally, the three last integrals of (24) vanish because of boundary conditions at the plate-porous interface (see Eqs. (25), (26) and (27)).

3. Numerical implementation

3.1. Rayleigh–Ritz approximation

The Rayleigh–Ritz discretization method is used to solve the problem for classical boundary conditions on the base plate. The solid displacements are discretized as

$$w(x,y,t)=\sum_{m=1}^{Mw}\sum_{n=1}^{Nw} qw_{mn}(t)\alpha_m(\xi)\alpha_n(\eta), \tag{42}$$

$$\psi_x(x,y,t)=\sum_{m=1}^{Mx}\sum_{n=1}^{Nx} qx_{mn}(t)\frac{\mathrm{d}\alpha_m}{\mathrm{d}\xi}(\xi)\alpha_n(\eta), \tag{43}$$

$$\psi_y(x,y,t)=\sum_{m=1}^{My}\sum_{n=1}^{Ny} qy_{mn}(t)\alpha_m(\xi)\frac{\mathrm{d}\alpha_n}{\mathrm{d}\eta}(\eta), \tag{44}$$

where qw_{mn}, qx_{mn}, qy_{mn} are the unknown coefficients; ξ and η are dimensionless space variables: $\xi=2x/a-1$, $\eta=2y/b-1$. The trial functions α are described in Section 3.2.

The acoustic pressure of the fluid phase is constructed from the expression of the transverse displacement w:

$$p(x,y,z,t)=\sum_{m=1}^{Mw}\sum_{n=1}^{Nw}\sum_{r=1}^{Rp} qp_{mnr}(t)\alpha_m(\xi)\alpha_n(\eta)p_r(z) \tag{45}$$

with

$$p_r(z)=\sum_{r=1}^{Rp}\cos\frac{r\pi(z-h_p/2)}{2h_m},\ r\ \text{odd} \tag{46}$$

Note that the used trial functions for the pressure are admissible in the sense that they satisfy the boundary conditions at $z=h_p/2$ and $z=h_p/2+h_m$: the derivative of the acoustic pressure is fixed to zero at the plate–porous interface (impervious condition), while the pressure is supposed to be zero at the porous–air interface (no fluid loading is implemented).

Table 1
Coefficients a_m, b_m, c_m and d_m of the functions set

Order m	Coefficient a_m	Coefficient b_m	Coefficient c_m	Coefficient d_m
1	$\pi/4$	$3\pi/4$	$\pi/4$	$3\pi/4$
2	$\pi/4$	$3\pi/4$	$-\pi/2$	$-3\pi/2$
3	$\pi/4$	$-3\pi/4$	$\pi/4$	$-3\pi/4$
4	$\pi/4$	$-3\pi/4$	$\pi/2$	$-3\pi/2$
$m>4$	$(m-4)\pi/2$	$(m-4)\pi/2$	$\pi/2$	$\pi/2$

3.2. Functions set

The functions set of Beslin and Nicolas [7] is used. This functions set, built from trigonometric functions, is a simple and easy way to handle various boundary conditions with both numerical stability and efficiency compared to other sets such as polynomials. The order of a $\alpha_m(\xi)$ function is not related to a power of ξ but to the number of oscillations of the trigonometric function. The functions are indefinitely derivable and only a low and constant number of basic operations is required to integrate matrices with no particular care of roundoff error.

The functions are of the form:

$$\alpha_m(\xi) = \sin(a_m\xi + b_m)\sin(c_m\xi + d_m) \tag{47}$$

with coefficients a_m, b_m, c_m and d_m defined in Table 1.

The selection of the basis functions used to describe w allows for fixing various boundary conditions for the base plate:

- free : functions of order m equal or greater than 1 are used ($m \geqslant 1$).
- simply supported: $m = 2, 4$ and $m \geqslant 5$.
- clamped: $m \geqslant 5$.

The whole functions set is used to approximate angles ψ_x and ψ_y to ensure a free rotation of the second layer.

Using this trigonometric set of functions, Eqs. (34), (39), (40) and (41) are written in terms of the unknown coefficients qw_{mn}, qx_{mn}, qy_{mn}. Once solved, the classical vibro-acoustic indicators of the problem are computed: quadratic velocity in the plate, quadratic velocity and pressure in the porous layer, dissipated powers in the two layers system [4].

4. Experiments

To validate the model, comparisons with complete three-dimensional poro-elastic finite element models and experimental data are presented below for various configurations.

Two complete models are used: MNS/Nova [6,12] involving linear elements and SuperNova [15] a hierarchical and parallel version of the first one. Both have been extensively validated. Results from these models are quite the same for each simulation so they will indifferently be referenced as "Complete model" in the figures.

4.1. Experimental set-up and numerical considerations

The experimental set-up is shown in Fig. 3. The porous layer is glued to an aluminium plate with a light spray specific glue or a thin double sided adhesive. To ensure that the observed vibration modification is due to the added material, several tests have been done. These measurements show that the adhesive layer's presence can affect the results. In particular, it must be kept to a minimum thickness. Air gap must also be avoided.

An electrodynamic shaker driven by a white noise signal excites the aluminium plate by a point force. The input force is measured by means of a force transducer. The transverse velocity of the plate is measured by a light accelerometer and integrated over time for thick plates (3.175 mm) or measured by a laser vibrometer for thinner plates (1.2 mm). The force and velocity signals are collected through a spectrum analyzer to calculate Frequency Response Functions (FRF) or estimate the mean quadratic velocity of the plate. Measurements have been done at 20°C, under 980 to 1000 mbar of static pressure with 15–20% of relative humidity.

Simulations were done using the following plan meshes to obtain convergences: 15 by 17 elements for the complete linear model, 2 by 2 elements with 6 orders per elements for the complete hierarchical model and one element with 14 orders of interpolation for the proposed simplified model. In the thickness of the poro-elastic media, 7 elements were used for the complete linear model, 1 element with order 8 for the complete hierarchical one and 1 element with order 2 for the simplified model's fluid phase (cf. Eq. (46)).

As previously mentioned, the material's moduli and structural damping are frequency dependent. Their quasistatic properties, measured following the method described by Langlois et al. [16], are used in the simulations. This will explain the rising differences between experimental and numerical data with increasing frequency.

The dimensions of the aluminium plates used and quasistatic properties of the two rather different foams tested are given in Tables 2 and 3.

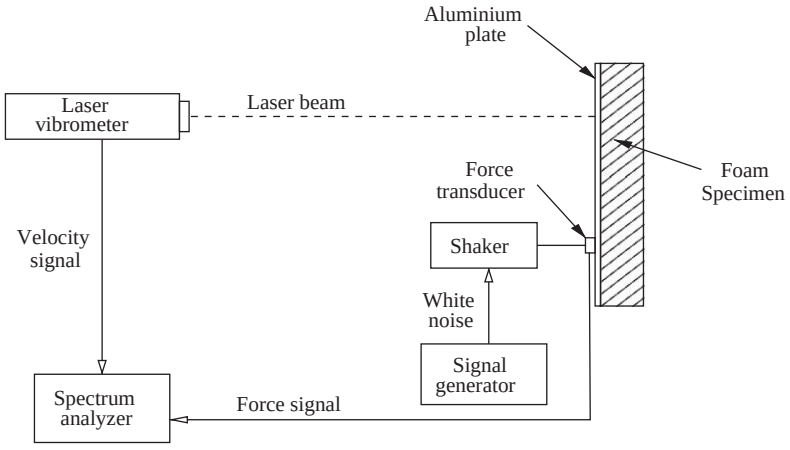

Fig. 3. Schema of the experimental set-up.

Table 2
Dimensions of the base aluminium plates

Plate	Length (mm)	Width (mm)	Thickness (mm)
1	350	220	1.2
2	420	480	3.175

Table 3
Properties of aluminium and foams

Material	E (N m^{-2})	ν	ρ_1 (kg m^{-3})	η	ϕ	σ (N s m^{-4})	α_∞	Λ (10^{-6} m)	Λ' (10^{-6} m)
Aluminium	$70 \cdot 10^9$	0.33	2740.00	0.001	—	—	—	—	—
Foam B	845 000	0.30	31.16	0.100	0.96	32 000	1.7	90	165
Foam M	160 000	0.44	8.35	0.060	0.99	12 600	1.0	78	192

4.2. Results

Fig. 4 presents the numerical results for a 1.2 mm simply supported aluminium plate treated by 20 mm of the polyurethane foam B. The contributions to the dissipated power of the different mechanisms are shown in Fig. 5. The results confirm earlier assumptions for this stiff foam:

- thermal dissipation is negligible in the low frequency range,
- the foam structural damping is the major dissipative phenomenon within the porous layer at low frequencies (it is maximum at the system resonances), and
- viscous dissipation remains weak in the frequency range of interest.

Figs. 6 and 7 show comparisons for a thicker plate (3.175 mm or $\frac{1}{8}$ in) with clamped or free boundary conditions. Good agreements are found between the complete 3-D and the simplified model calculations for these three different cases in the whole frequency range.

Comparisons between models and experimentations can be done with a few number of FRF. Fig. 8 shows an estimation of the mean quadratic velocity for a 3.175 mm aluminium plate with 25.4 mm (1 in) of the soft melamine foam M using an average of 6 FRF. The point force is at coordinates (390 mm; 120 mm), measurement points are reported in Table 4. A good agreement is again found between measurements and the simplified model although the material is supposed to be isotropic and its elastic parameters are considered constant in frequency.

4.3. Limitations of the model

To illustrate the limitations of the proposed model, Fig. 9 shows the results for an 3.175 mm aluminium plate treated by 76.2 mm (3 in) of the M foam. Below 350 Hz the numerical results agree well in frequency and amplitude. Above 350 Hz the damping is underestimated.

This frequency corresponds to the first quarter wavelength frequency resonance of the frame [2]. Above 350 Hz, the constant transverse displacement assumption over the multilayer thickness is no more valid, thus fixing an upper frequency limit to the proposed simplified model (one

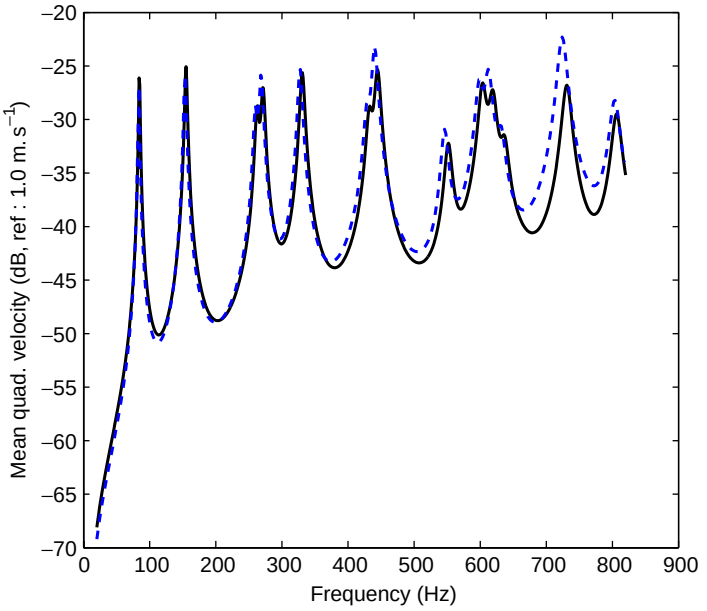

Fig. 4. Mean quadratic velocity of a 1.2 mm simply supported aluminium plate backed with 20 mm of foam B. ——: Simplified model, - - -: Complete model.

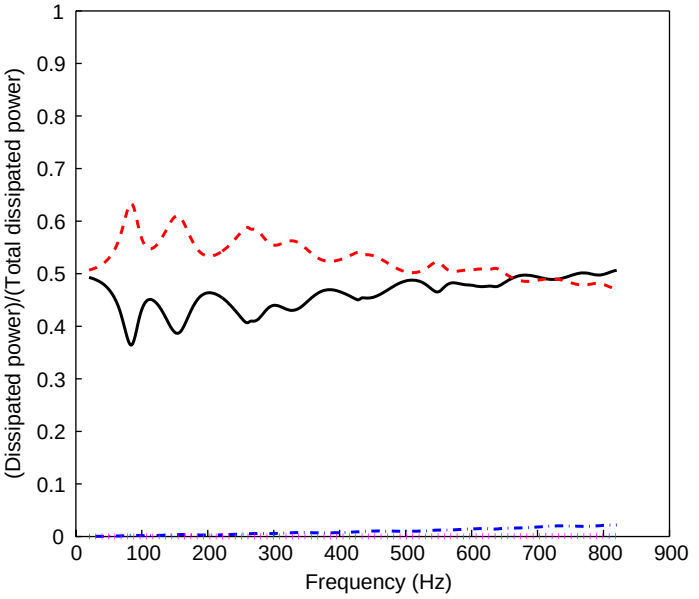

Fig. 5. Dissipation mechanisms distribution for a 1.2 mm simply supported aluminium plate treated with 20 mm of foam B. ——: Structural damping (plate), - - -: Structural damping (foam), -·-·-: Viscous effects, ·····: Thermal effects. Thermal dissipation is too close to zero to be seen clearly on this scale.

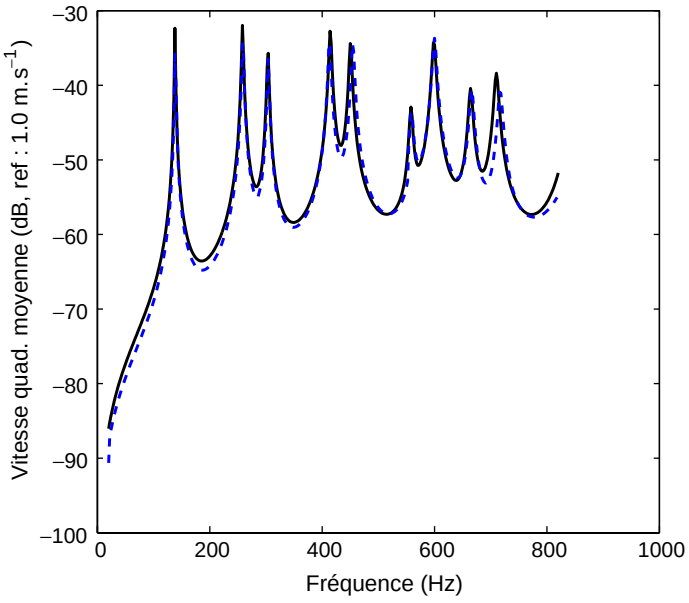

Fig. 6. Mean quadratic velocity of a 3.175 mm (1/8″) clamped aluminium plate backed with 20 mm of foam B. ——: Simplified model, - - -: Complete model.

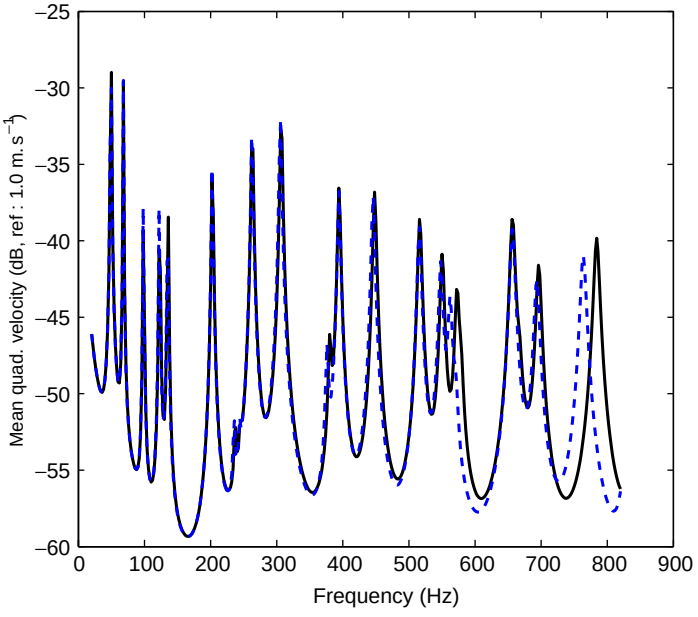

Fig. 7. Mean quadratic velocity of a 3.175 mm free aluminium plate backed with 20 mm of foam B. ——: Simplified model, - - -: Complete model.

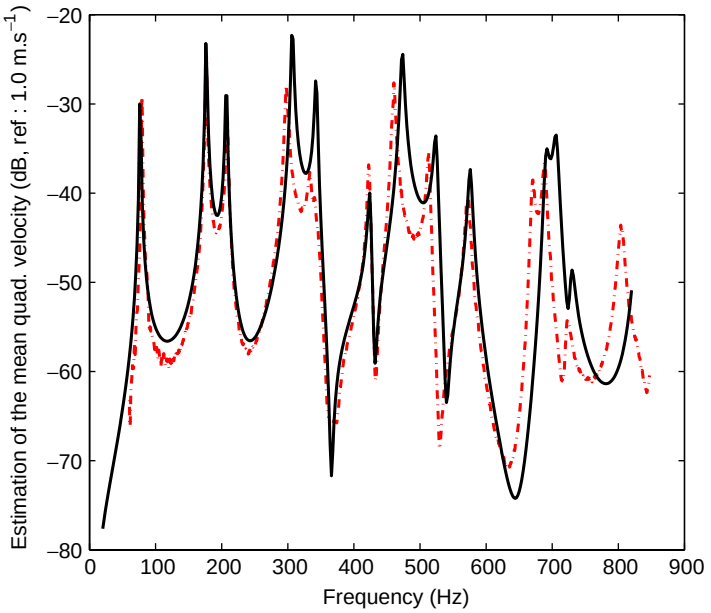

Fig. 8. Mean quadratic velocity of a 3.175 mm simply supported aluminium plate backed with 25.4 mm (1″) of foam M. ——: Simplified model simulation, -·-·-: Measurements.

Table 4
FRF measurement points for Fig. 8

Point	Coordinates (mm)
1	(90; 90)
2	(90; 270)
3	(210; 120)
4	(210; 330)
5	(330; 210)
6	(330; 390)

should keep in mind that the purpose of this work is to reduce computation time for plate-porous configuration systems, not to test efficiency of high dissipative porous materials). A complete three-dimensional poro-elastic finite element model is required to calculate well the material's solid phase displacements and the viscous dissipation associated to the new relative displacements of the foam's two phases (cf. Fig. 10).

In the previous cases, the first quarter wavelength frequency resonances occur beyond the upper limit of the experimental frequency.

4.4. *Performances*

Due to slow convergence of linear poro-elastic elements, accurate prediction requires about 5000 degrees-of-freedom (DOF) for a complete classical linear finite element code. This number of

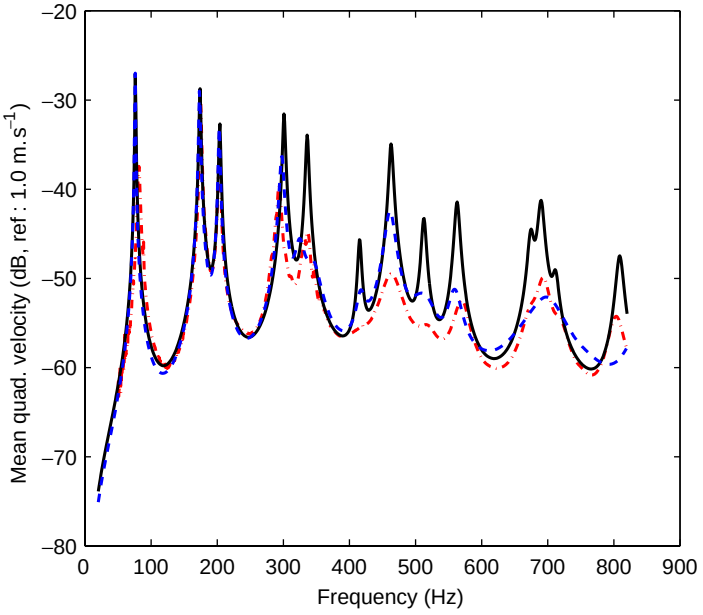

Fig. 9. Mean quadratic velocity of a 3.175 mm simply supported aluminium plate backed by 76.2 mm (3″) of foam M. ——: Simplified model, - - -: Complete model, -·-·-: Measurements.

DOF falls to 2000 using a complete hierarchical finite element model and reduces even further to 600 for the proposed simplified method. However, it must be noted that the numerical codes do not use the same plate models: the 3-D linear finite element model uses membrane displacements and Kirchhoff quadrangle element with bubbles functions and static condensation [17]. The 3-D hierarchical code uses Mindlin assumption with MSC/Probe [18] functions set.

Noting that the matrices terms are frequency dependent, the numerical problem cannot be solve easily by a modal approach [19]. A direct solver is thus used to obtain the results for 800 frequency points. In term of time usage on a 1 GHz 80686 CPU, the complete linear model calculation time is about 20 h, the hierarchical model and simplified model ones are about 1 h and 2 min, respectively (for a simple plate problem, calculation times are: 2 h and 30 min, 10 min and 20 s).

5. Conclusions

The proposed simplified model to simulate the vibration behaviour of an elastic plate backed by a polymeric foam has been numerically and experimentally validated for two rather different foams (a stiff and a soft one) and various boundary conditions.

This model is relevant when the thickness of the porous material allows verification of the constant transverse displacement over the multilayer assumption. Consequently it cannot be used to predict the mechanical behaviour of high thickness foams bonded onto metal plates beyond the first quarter wavelength frequency resonance. However, the model serves its purpose by reducing

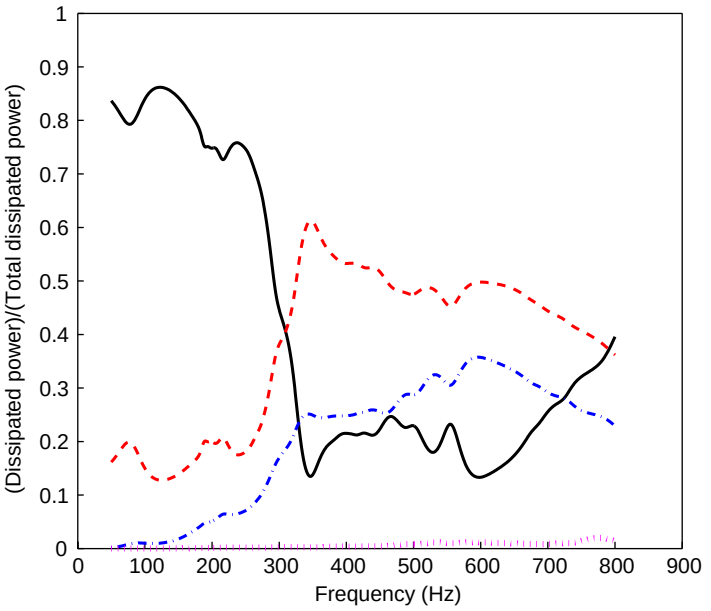

Fig. 10. Dissipation mechanisms distribution for a 3.175 mm simply supported aluminium plate treated with 76.2 mm of foam M. ——: Structural damping (plate), - - -: Structural damping (foam), -·-·-: Viscous effects, ·····: Thermal effects.

the computation time and memory usage for plate-porous configurations and offers an efficient tool to quickly characterize the mechanical properties of thin foam samples in a low frequency band by an inverse method.

A point worth mentioning is the fact that the poro-elastic layer is modelled as an isotropic material although this is not the case for most of the foams. Nevertheless an acceptable correlation is found between simulations and experimental data. An extension to anisotropic foams would be an interesting complement to the present study.

Acknowledgements

The authors are grateful to Manuel Etchessahar and Nicolas Dauchez for their friendly supports and the French and Quebecer Ministères Des Relations Internationales for their financial assistance.

References

[1] M.A. Biot, The theory of propagation of elastic waves in a fluid-satured porous solid. I. Low frequency range. II. Higher frequency range, *Journal of the Acoustical Society of America* 28 (1956) 168–191.

[2] J.F. Allard, *Propagation of Sound in Porous Media: Modeling Sound Absorbing Materials*, Chapman & Hall, London, 1993.

[3] N. Dauchez, S. Sahraoui, N. Atalla, Dissipation mechanisms in a porous layer bonded onto a plate, *Journal of Sound and Vibration* 265 (2003) 437–449.
[4] S. Rigobert, Modélisation par Élément Finis des Systèmes Élasto-poro-acoustiques Couplés, Ph.D. Thesis, University of Sherbrooke(Qc), Canada and INSA de Lyon, France, 2001.
[5] M. Etchessahar, S. Sahraoui, B. Brouard, Bending vibrations of a rectangular poroelastic plate, *Comptes Rendus de l'Académie des Sciences de Paris—Series IIB—Mechanics* 329 (2001) 615–620.
[6] N. Atalla, R. Panneton, P. Debergue, A mixed displacement-pressure formulation for poroelastic materials, *Journal of the Acoustical Society of America* 104 (1998) 1444–1452.
[7] O. Beslin, J. Nicolas, A hierarchical functions set for predicting very high order plate bending modes with any boundary conditions, *Journal of Sound and Vibration* 202 (1997) 633–655.
[8] D.L. Johnson, J. Koplik, R. Dashen, Theory of dynamic permeability and tortuosity in fluid-saturated porous media, *Journal of Fluid Mechanics* 176 (1987) 379–402.
[9] Y. Champoux, J.-F. Allard, Dynamic tortuosity and bulk modulus in air-saturated porous media, *Journal of Applied Physics* 70 (1991) 1975–1979.
[10] C. Depollier, J.-F. Allard, W. Lauriks, Biot theory and stress-strain equations in porous sound absorbing materials, *Journal of the Acoustical Society of America* 84 (1988) 2277–2279.
[11] P. Lemarinier, Propagation du Son à Basses Fréquences Audibles (30–5000 Hz) dans les Mousses et une Laine de Verre Saturée d'Air, Ph.D. Thesis, Université du Maine, Le Mans, France, 1997.
[12] N. Atalla, M.A. Hamdi, R. Panneton, Enhanced weak formulation for the mixed $(\mathbf{u}, p)$ poroelastic equations, *Journal of the Acoustical Society of America* 109 (2001) 3065–3068.
[13] A.E.H. Love, On the small free vibrations and deformations of elastic shells, *Philosophical Transactions of the Royal Society (London)* A (1888) 491–549.
[14] R.D. Mindlin, Influence of rotatory inertia and shear on flexural motions of isotropic, elastic plates, *Journal of Applied Mechanics* 18 (1951) 31–38.
[15] C. Langlois, Modelling Vibro-acoustic Problems with Finite Elements, Master's Thesis, University of Sherbrooke(Qc), Canada, 2003.
[16] C. Langlois, R. Panneton, N. Atalla, Polynomial relations for quasi-static mechanical characterization of isotropic poroelastic materials, *Journal of the Acoustical Society of America* 110 (2001) 3032–3040.
[17] R.J. Guyan, Reduction of stiffness and mass matrices, *Journal of the American Institute of Aeronautics and Astronautics* 3 (1965) 380.
[18] R.H. MacNeal, *Finite Elements: Their Design and Performance*, Marcel Dekker, New York, 1993.
[19] O. Dazel, F. Sgard, C.-H. Lamarque, N. Atalla, An extension of complex modes for the resolution of finite-element poroelastic problems, *Journal of Sound and Vibration* 253 (2002) 421–445.